Supporting information

Enhanced Low-Temperature Activity and Hydrothermal Stability of Ce-Mn Oxide-Modified Cu-SSZ-39 Catalysts for NH_3-SCR of NO_x

Ahui Tang[1], Fuzhen Yang[1], Ying Xin[1,*], Xiaoli Zhu[1], Long Yu[1], Shuai Liu[1], Dongxu Han[1], Junxiu Jia[1], Yaning Lu[1], Zhenguo Li[2], Zhaoliang Zhang[1]

[1]School of Chemistry and Chemical Engineering, Shandong Provincial Key Laboratory of Fluorine Chemistry and Chemical Materials, University of Jinan, Jinan 250022, China

[2]National Engineering Laboratory for Mobile Source Emission Control Technology, China Automotive Technology & Research Center Co., Ltd., Tianjin 300300, China

Corresponding authors:

Ying Xin: chm_xiny@ujn.edu.cn; Tel.: +86-531-89736032

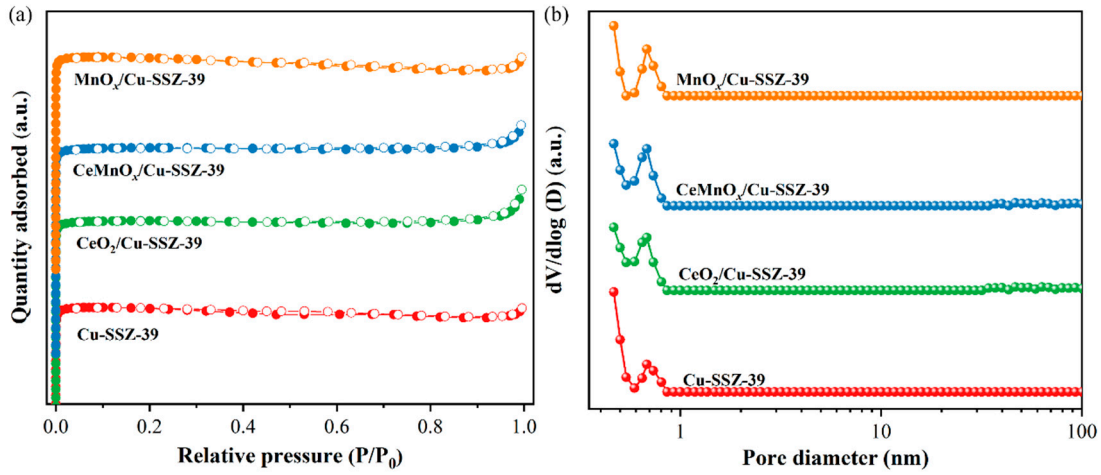

Figure S1. N_2 adsorption/desorption isotherms (a) and pore size distribution curves (b) of Cu-SSZ-39, CeO_2/Cu-SSZ-39, $CeMnO_x$/Cu-SSZ-39, and MnO_x/Cu-SSZ-39 catalysts.

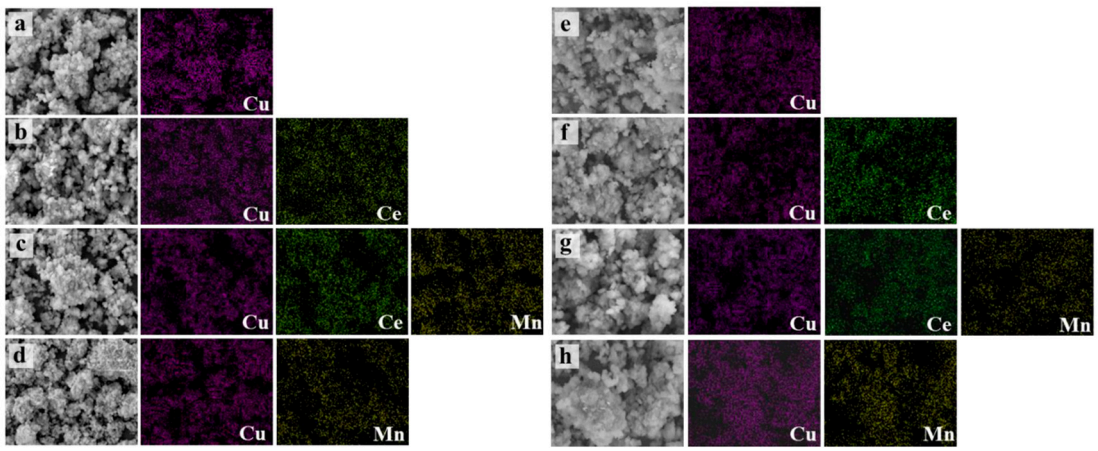

Figure S2. SEM images and Cu, Ce, Mn element EDS mappings of Cu-SSZ-39 (a,e), CeO_2/Cu-SSZ-39 (b,f), $CeMnO_x$/Cu-SSZ-39 (c,g), and MnO_x/Cu-SSZ-39 (d,h) catalysts: (a–d) fresh and (e–h) hydrothermally aged samples.

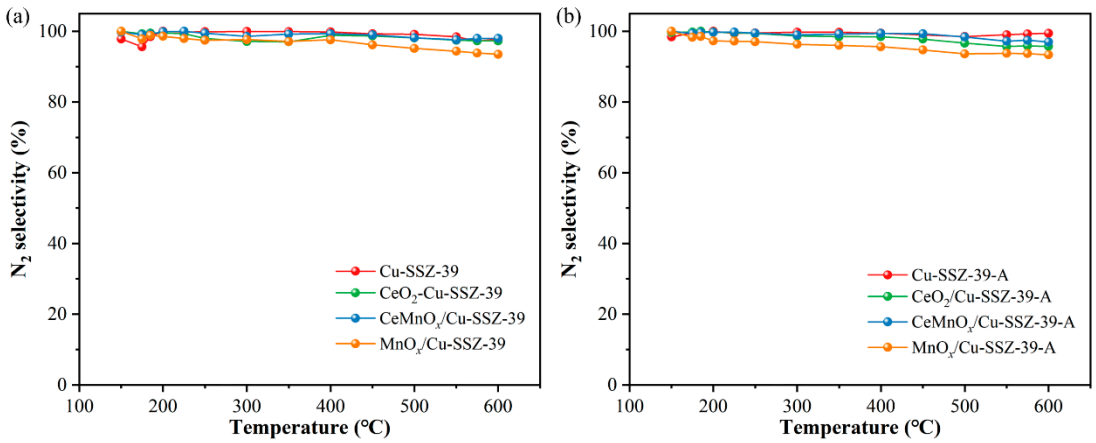

Figure S3. N_2 selectivity of Cu-SSZ-39, CeO_2/Cu-SSZ-39, $CeMnO_x$/Cu-SSZ-39, and MnO_x/Cu-SSZ-39 catalysts: (a) fresh samples and (b) hydrothermal aged samples.

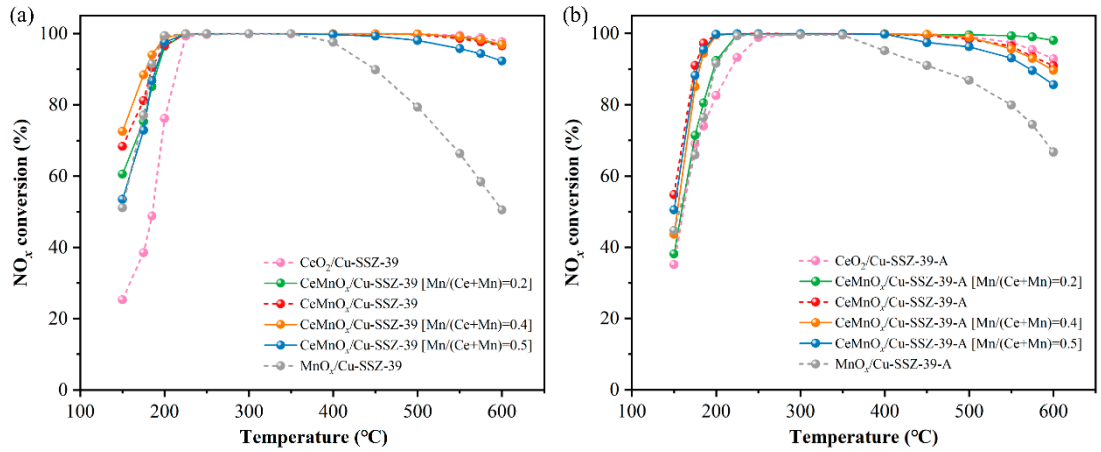

Figure S4. NO_x conversion of CeO_2/Cu-SSZ-39, $CeMnO_x$/Cu-SSZ-39 [Mn/(Ce + Mn) = 0.2], $CeMnO_x$/Cu-SSZ-39, $CeMnO_x$/Cu-SSZ-39 [Mn/(Ce + Mn) = 0.4], $CeMnO_x$/Cu-SSZ-39 [Mn/(Ce + Mn) = 0.5], and MnO_x/Cu-SSZ-39 catalysts: (a) fresh samples and (b) hydrothermally aged samples.

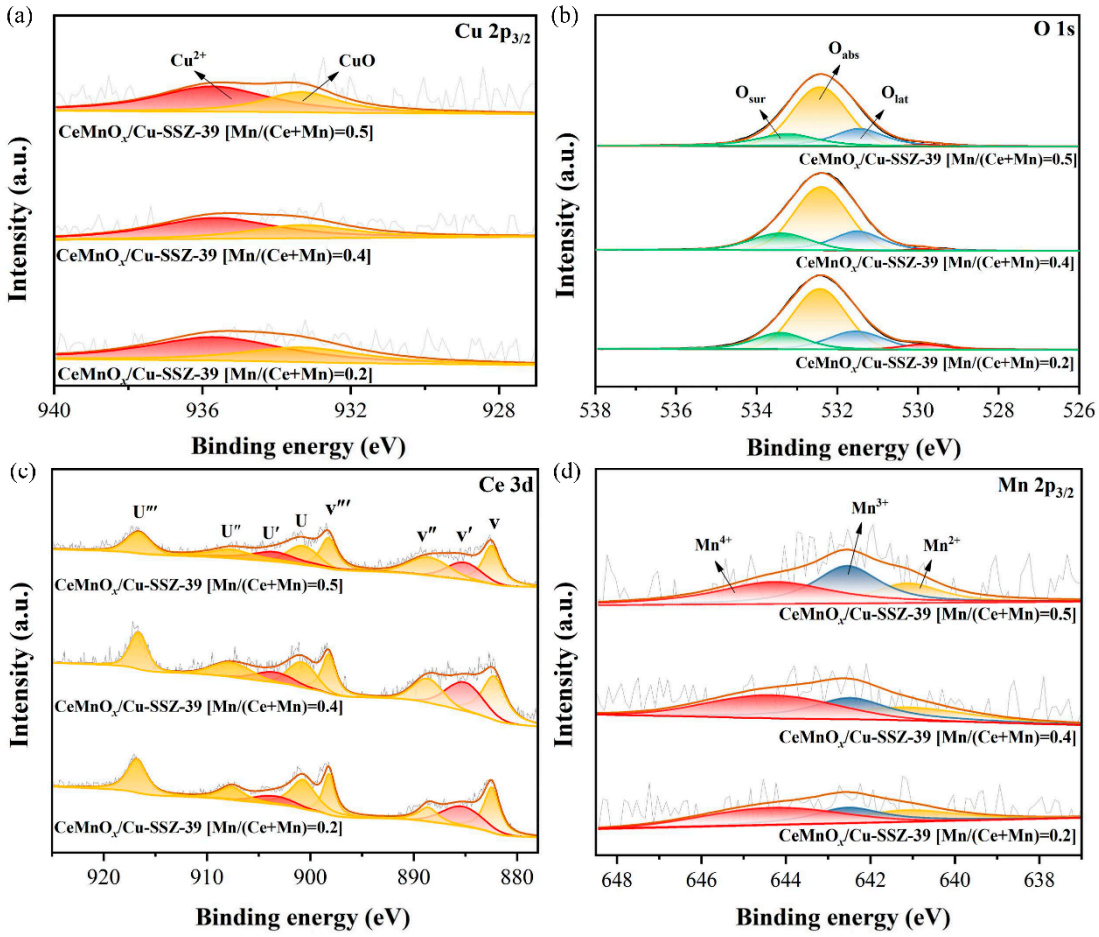

Figure S5. XPS spectra of Cu $2p_{3/2}$ (a) (gray line was assigned to the original data, dark yellow line was assigned to the fitting curve); O 1s (b) (black line was assigned to the original data, dark yellow line was assigned to the fitting curve); Ce 3d (c) (gray line was assigned to the original data, dark yellow line was assigned to the fitting curve); and Mn $2p_{3/2}$ (d) (gray line was assigned to the original data, dark yellow line was assigned to the fitting curve) of $CeMnO_x$/Cu-SSZ-39 [Mn/(Ce + Mn) = 0.2], $CeMnO_x$/Cu-SSZ-39 [Mn/(Ce + Mn) = 0.4], and $CeMnO_x$/Cu-SSZ-39 [Mn/(Ce + Mn) = 0.5] catalysts.

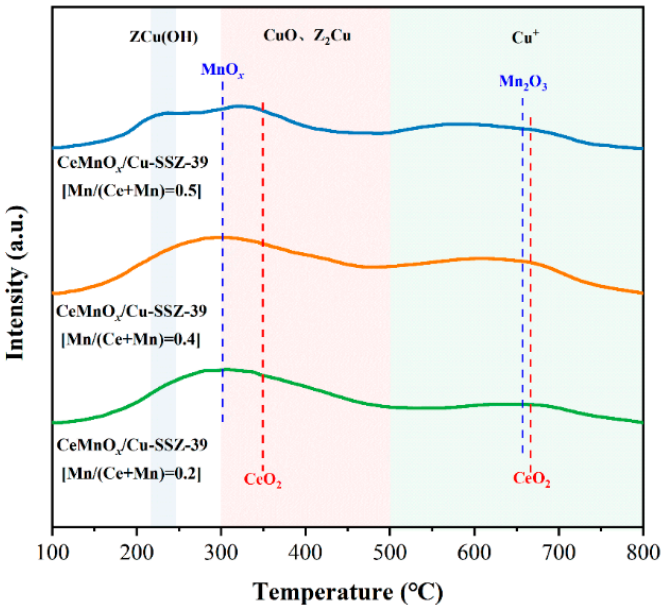

Figure S6. H_2-TPR profiles of $CeMnO_x$/Cu-SSZ-39 [Mn/(Ce + Mn) = 0.2], $CeMnO_x$/Cu-SSZ-39 [Mn/(Ce + Mn) = 0.4], and $CeMnO_x$/Cu-SSZ-39 [Mn/(Ce + Mn) = 0.5] catalysts.

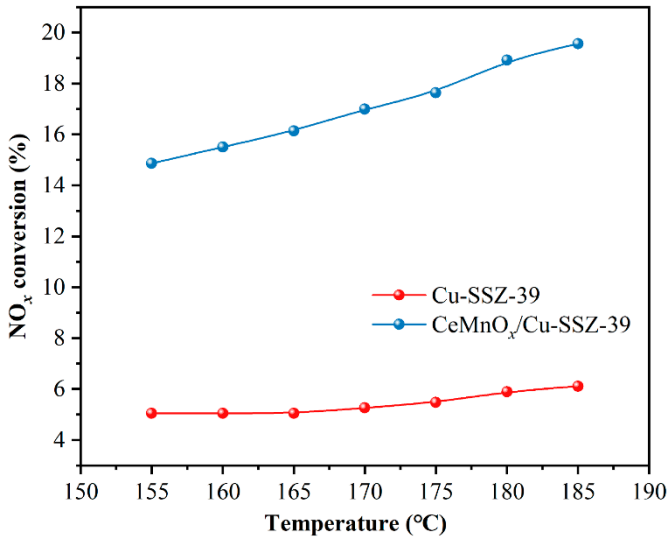

Figure S7. Kinetic catalytic performances of Cu-SSZ-39 and $CeMnO_x$/Cu-SSZ-39 catalysts.

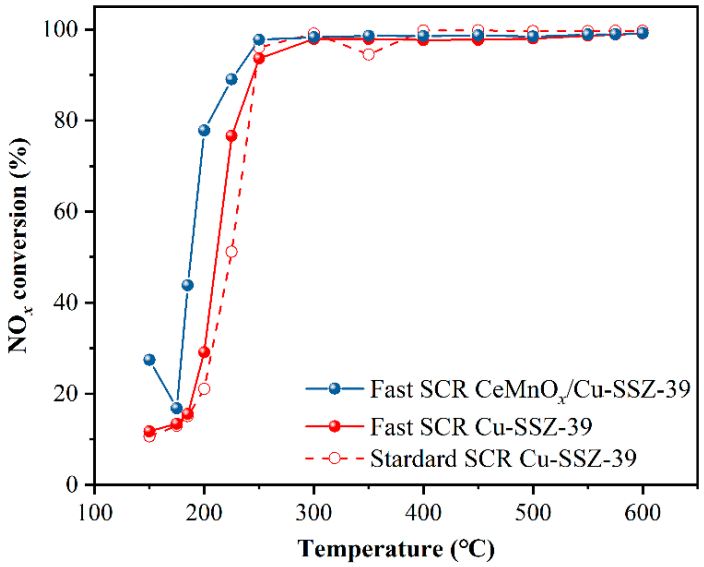

Figure S8. NO_x conversion under fast SCR condition in Cu-SSZ-39 and $CeMnO_x$/Cu-SSZ-39 catalysts.

Table S1. Cu $2p_{3/2}$, O 1s, Ce 3d, and Mn $2p_{3/2}$ XPS analysis of the catalysts.

Sample	Cu (%)		O (%)			Ce (%)		Mn (%)		
	Cu^{2+}	CuO	O_{sur}	O_{ads}	O_{lat}	Ce^{3+}	Ce^{4+}	Mn^{2+}	Mn^{3+}	Mn^{4+}
$CeMnO_x$/Cu-SSZ-39 [Mn/(Ce + Mn) = 0.2]	64.8	35.2	19.1	59.1	21.7	20.0	80.0	28.1	29.9	42.0
$CeMnO_x$/Cu-SSZ-39 [Mn/(Ce + Mn) = 0.4]	65.2	34.8	18.5	59.3	22.1	22.3	77.7	27.8	32.7	39.5
$CeMnO_x$/Cu-SSZ-39 [Mn/(Ce + Mn) = 0.5]	64.7	35.3	18.8	59.1	22.1	22.7	77.3	25.3	36.7	38.0